

Duality symmetries and effective dynamics in disordered hopping models

Robert L. Jack

Department of Physics, University of Bath, Bath BA2 7AY, UK

Peter Sollich

King's College London, Department of Mathematics, London WC2R 2LS, UK

Abstract. We identify a duality transformation in one-dimensional hopping models that relates propagators in general disordered potentials related by an up-down inversion of the energy landscape. This significantly generalises previous results for a duality between trap and barrier models. We use the resulting insights into the symmetries of these models to develop a real-space renormalisation scheme that can be implemented computationally and allows rather accurate prediction of propagation in these models. We also discuss the relation of this renormalisation scheme to earlier analytical treatments.

1. Introduction

The motion of particles in disordered environments is important in many contexts, from glass-forming liquids and colloids [1, 2], to biomolecules moving in the crowded environment of the cell [3], to electrical properties of disordered materials [4]. In this article, we discuss subdiffusive propagation in simple one-dimensional models. While the case of one-dimensional motion may seem simplistic, it is relevant for a variety of model systems: from early studies of electrical transport [4] to recently-defined models of glassy behaviour [5], and also to the motion of defects in disordered magnets, to disordered elastic chains and to networks of resistors and capacitors (see [6, 7, 8, 9] for reviews).

The results that we will present are based around a duality symmetry which relates pairs of discrete one-dimensional models. In a previous study [10], we showed that motion in apparently disparate models can be related exactly, at fixed disorder. Here we generalise those results to a much wider range of hopping models, by treating their master equations in a simple operator formalism. Based on the symmetries of the problem, we also introduce a real-space renormalisation scheme in the spirit of that of le Doussal, Monthus and Fisher [11]: our scheme is implemented computationally and allows rapid prediction of the propagation in these energy landscapes for fixed disorder, at low computational cost.

The central feature of the renormalisation scheme is that on a given time scale, we have a procedure for decomposing the system into effective trap and barrier regions. Particles within trap regions equilibrate there, while those in barrier regions decay into the effective traps. The duality symmetry relates trap and barrier regions of pairs of models, and demands that they be treated on an equal footing within the renormalisation scheme. In some sense, the renormalisation scheme is connected with the ideas of an energy landscape in these disordered systems [12], but we note that all properties of the energy landscape are here derived directly from the master operator of the stochastic dynamics. In this sense, our scheme allows the energy landscape to be derived from the dynamical rules of the system: this is the opposite of the usual situation in which thermodynamic properties are used to infer the routes by which dynamical processes take place. Thus, while our results are clearly restricted to a very simple class of models, it is natural to ask if they might be generalised to higher-dimensional energy landscapes.

The form of the paper is as follows: in Sec. 2 we define our models and give the duality relation between their master operators. The consequences of the duality relation for propagation in these models are discussed in Sec. 3. In Sec. 4 we explain our effective dynamics scheme; Sec. 5 contains numerical results for specific ensembles of disordered models; and Sec. 6 closes with a brief summary and some open questions.

2. Models and duality relations

We define a disordered one-dimensional hopping model in terms of rates for hops from site i to sites $i - 1$ and $i + 1$, which we denote by ℓ_i and r_i respectively. Let $p_i(t)$ be the probability that a particle occupies site i at time t : the master equation is then

$$\frac{\partial}{\partial t} p_i(t) = \ell_{i+1} p_{i+1}(t) + r_{i-1} p_{i-1}(t) - (\ell_i + r_i) p_i(t). \quad (1)$$

For concreteness, we consider a periodic chain of N sites, but we are primarily concerned with propagation of particles on infinite chains: that is, we consider the

limit of large N before any limit of large time. In this limit, propagators will be independent of the choice of boundary conditions. We also discuss finite chains with reflecting and absorbing boundaries in section 2.1 below.

We use an operator notation where the ket $|i\rangle$ represents the state with the particle on site i , normalised so that $\langle i|j\rangle = \delta_{ij}$. Then, defining the state $|P(t)\rangle = \sum_i p_i(t)|i\rangle$, the master equation can be written as $\frac{\partial}{\partial t}|P(t)\rangle = W^{(1)}|P(t)\rangle$ with

$$W^{(1)} = \sum_{i=1}^N [\ell_i|i-1\rangle + r_i|i+1\rangle - (l_i + r_i)|i\rangle] \langle i| \quad (2)$$

$$= \sum_{i=1}^N (|i+1\rangle - |i\rangle)(r_i\langle i| - \ell_{i+1}\langle i+1|). \quad (3)$$

In this section, and wherever we consider systems with periodic boundaries, site $i = N + 1$ is equivalent to site 1 and site 0 is equivalent to site N . This allows terms to be rearranged as e.g. in going from (2) to (3) above.

We initially focus on an important special case: we assume that all rates are finite and that $\prod_i \ell_i = \prod_i r_i$. This ensures that all currents vanish in the long-time limit of the system. Under this assumption, we associate an energy with each site, measured *downwards* from an arbitrary baseline and determined through $\ell_{i+1}e^{E_{i+1}} = r_i e^{E_i}$. Then, the model respects detailed balance with respect to the distribution $p_i^{\text{eq}} = e^{E_i} / (\sum_r e^{E_r})$, where the sum runs over all sites. With this sign convention, a site with large positive E_i has a large Gibbs weight. The reason for this choice will become clear below.

We now discuss general duality relations between pairs of hopping models. To this end, we re-parameterise the transition rates ℓ_i and r_i by defining transition state energies $E_{i+\frac{1}{2}}$ associated with the links between sites:

$$\ell_i = e^{-(E_{i-\frac{1}{2}} + E_i)}, \quad r_i = e^{-(E_{i+\frac{1}{2}} + E_i)} \quad (4)$$

(Note that site energies E_i and transition state energies $E_{i+\frac{1}{2}}$ are measured with respect to separate arbitrary baselines, so they do not necessarily have to be positive; but an interpretation in terms of activated hopping processes becomes problematic unless $E_i + E_{i\pm\frac{1}{2}} > 0$.)

Two subclasses of these general hopping models have been studied quite extensively in the past [4, 6, 8, 10, 13, 14, 15, 16]. The first subclass is the (pure) trap model, which is the case $E_{i+\frac{1}{2}} = 0$ for all i , with the E_i being independent and identically distributed (i.i.d.); the second is the (pure) barrier model, which has $E_i = 0$ for all i , with the $E_{i+\frac{1}{2}}$ being i.i.d. A duality between pure trap and pure barrier models was discussed in [10], which we now generalise. The duality relation involves an inversion of the potential, which swaps the meaning of transition state energies and site energies: the various definitions are illustrated in Fig. 1. To present this relation, we define an alternative representation of the general hopping model, in which sites have indices $i + \frac{1}{2}$ (throughout this article, i is always an integer). The hopping rate from $i - \frac{1}{2}$ to $i + \frac{1}{2}$ is R_i and the rate for the reverse process is L_i . The master equation for this process has a similar representation in terms of state vectors $|i + \frac{1}{2}\rangle$, with a master operator

$$W^{(1/2)} = \sum_{i=1}^N (|i + \frac{1}{2}\rangle - |i - \frac{1}{2}\rangle) (R_i\langle i - \frac{1}{2}| - L_i\langle i + \frac{1}{2}|). \quad (5)$$

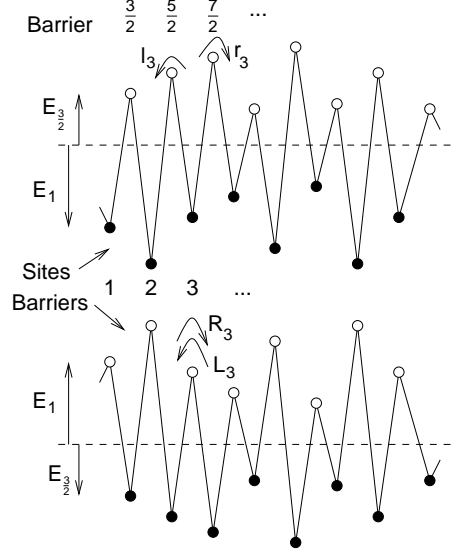


Figure 1. (Top) Illustration of an ‘energy landscape’, defined by supplementing the site energies E_i by transition state energies $E_{i+\frac{1}{2}}$. The rate for hopping from a site is related to the sum of the site energy (measured downwards as shown) and the adjacent transition state energy (measured upwards). (Bottom) On inversion of the potential, the transition state energies become energies of new sites with half-integer indices: transition rates between these sites are controlled by the energies E_i which now have an interpretation as transition state energies.

If we choose $R_i = r_i$ and $L_i = \ell_{i+1}$, then $W^{(1/2)}$ describes the same model as $W^{(1)}$, up to a simple relabelling of sites (site i in $W^{(1)}$ is mapped to site $i - \frac{1}{2}$ in $W^{(1/2)}$). To describe instead the inverted potential of Fig. 1, we choose

$$R_i = e^{-(E_i + E_{i-\frac{1}{2}})} = \ell_i, \quad L_i = e^{-(E_i + E_{i+\frac{1}{2}})} = r_i \quad (6)$$

With these definitions, the duality relation takes a simple form: we define operators

$$S = \sum_{i=1}^N (|i+1\rangle - |i\rangle) \langle i + \frac{1}{2}| e^{-E_{i+\frac{1}{2}}} \quad (7)$$

$$= \sum_{i=1}^N |i\rangle \left(e^{-E_{i-\frac{1}{2}}} \langle i - \frac{1}{2}| - e^{-E_{i+\frac{1}{2}}} \langle i + \frac{1}{2}| \right) \quad (8)$$

and

$$\bar{S} = \sum_{i=1}^N (|i + \frac{1}{2}\rangle - |i - \frac{1}{2}\rangle) \langle i| e^{-E_i} \quad (9)$$

$$= \sum_{i=1}^N |i + \frac{1}{2}\rangle (\langle i| e^{-E_i} - \langle i+1| e^{-E_{i+1}}). \quad (10)$$

Hence, by combining the first expression (7) for S with the second expression (10) for \bar{S} , and *vice versa*, one verifies that

$$W^{(1)} = S\bar{S}, \quad W^{(1/2)} = \bar{S}S. \quad (11)$$

It follows that

$$\overline{S}W^{(1)} = W^{(1/2)}\overline{S}, \quad (12)$$

and that

$$W^{(1)}S = SW^{(1/2)}. \quad (13)$$

These two relations express the key duality between the two master operators from which all our other results are derived. They imply, for example, that $W^{(1)}$ and $W^{(1/2)}$ have the same spectrum of eigenvalues: if $|\psi\rangle$ is a right eigenvector of $W^{(1/2)}$ then $S|\psi\rangle$ is a right eigenvector of $W^{(1)}$ with the same eigenvalue. The exception is the singular case where $S|\psi\rangle = 0$, which can happen only when the eigenvalue is zero. An analogous argument can be made in the other direction, showing overall that the nonzero eigenvalues and associated eigenvectors of $W^{(1)}$ and $W^{(1/2)}$ are in one-to-one correspondence with each other.

In fact, the structure of (11) occurs in the context of supersymmetric field theories (for a discussion of supersymmetry in the language of operators, applied to energy landscapes, see [17]; for a more general introduction, see [18]). These hopping models are very simple examples of supersymmetric partners: the spaces $\{|i\rangle\}$ and $\{|i + \frac{1}{2}\rangle\}$ can be interpreted as zero- and one-fermion subspaces of a generalised superspace. Acting to the right, the operator S annihilates all elements of $\{|i\rangle\}$ and \overline{S} annihilates all elements of $\{|i + \frac{1}{2}\rangle\}$ so $S^2 = \overline{S}^2 = 0$: these operators are the supercharges of the theory. We can then write $W^{(1)} + W^{(1/2)} = S\overline{S} + \overline{S}S$ which allows us to identify the two models as supersymmetric partners.

It is also instructive to consider the continuum limit of our lattice model. Assume that the lattice spacing is a , so that the position of site i is $x_i = ia$. We define continuous functions $V_1(x)$ and $V_{1/2}(x)$ and take $E_i = V_1(x_i)$ and $E_{i+\frac{1}{2}} = V_{1/2}(x_{i+\frac{1}{2}})$. Within the continuum limit, we represent the superspace explicitly, using a basis $|x, n\rangle$, where x is the position and $n = 0, 1$ distinguishes the zero- and one-fermion subspaces. That is, taking fermionic operators c, c^\dagger with $c^2 = (c^\dagger)^2 = 0$ and $cc^\dagger + c^\dagger c = 1$, we take $c|x, 0\rangle = 0$ and $|x, 1\rangle = c^\dagger|x, 0\rangle$. To make contact with the basis used for the lattice model, we identify $|i\rangle$ with $|x_i, 0\rangle$ and $|i + \frac{1}{2}\rangle$ with $|x_i, 1\rangle$. If we then divide S and \overline{S} by a and take the lattice spacing to zero, we arrive at

$$S = c \frac{d}{dx} e^{-V_{1/2}(x)}, \quad \overline{S} = c^\dagger \frac{d}{dx} e^{-V_1(x)} \quad (14)$$

The master (or Fokker-Planck) operators follow as

$$\begin{aligned} W^{(1)} &= S\overline{S} = cc^\dagger \frac{d}{dx} e^{-V_{1/2}(x)} \frac{d}{dx} e^{-V_1(x)}, \\ W^{(1/2)} &= \overline{S}S = c^\dagger c \frac{d}{dx} e^{-V_1(x)} \frac{d}{dx} e^{-V_{1/2}(x)} \end{aligned} \quad (15)$$

This makes it obvious that the duality just swaps the trap and barrier parts of the potential, i.e. inverts the energy landscape. In the case without thermal activation, which corresponds to $V_{1/2} = -V_1 = V$, the duality reduces to the standard one for diffusion in the potentials V and $-V$. One part of this duality was used recently in [19] to map boundary-driven steady states with current to current-free equilibrium states. Briefly, if $P(x)$ is a steady state probability distribution of $W^{(1)}$ in the presence of a boundary field so that $W^{(1)}|P(x), 0\rangle = 0$, then $|\tilde{P}(x), 1\rangle = \overline{S}|P(x), 0\rangle$ obeys $S|\tilde{P}(x), 1\rangle = 0$. Thus, $|\tilde{P}(x), 1\rangle$ is a steady state of $W^{(1/2)}$, but the current in this state is $e^V (d/dx) e^{-V} |\tilde{P}(x), 1\rangle = e^V c^\dagger S |\tilde{P}(x), 1\rangle = 0$. The same approach also works

on the lattice, and indeed the rate transformation (182) in Ref. [19] is the same as our (6).

The total master operator combining the dynamics in the zero and one-fermion spaces can be made Hermitian by a standard similarity transformation: with $D = cc^\dagger e^{\frac{1}{2}V_1(x)} + c^\dagger c e^{\frac{1}{2}V_{1/2}(x)}$ one has

$$H = D^{-1}(W^{(1)} + W^{(1/2)})D \\ = cc^\dagger e^{-\frac{1}{2}V_1(x)} \frac{d}{dx} e^{-V_{1/2}(x)} \frac{d}{dx} e^{-\frac{1}{2}V_1(x)} + c^\dagger c e^{-\frac{1}{2}V_{1/2}(x)} \frac{d}{dx} e^{-V_1(x)} \frac{d}{dx} e^{-\frac{1}{2}V_{1/2}(x)} \quad (16)$$

Using $cc^\dagger = 1 - c^\dagger c$ to extract the extra contribution from the one-fermion subspace, one can simplify this to

$$H = e^{-\frac{1}{2}V_1(x)} \frac{d}{dx} e^{-V_{1/2}(x)} \frac{d}{dx} e^{-\frac{1}{2}V_1(x)} \\ - c^\dagger c e^{-V_1(x) - V_{1/2}(x)} \left[\frac{1}{4}(V_1'(x)^2 - V_{1/2}'(x)^2) - \frac{1}{2}(V_1''(x) - V_{1/2}''(x)) \right] \quad (17)$$

For the ‘standard’ case with uniform diffusion constant $V_{1/2} = -V_1 = V$, the one-fermion term simplifies to $-c^\dagger c V''(x)$ and this is exactly the term that was used e.g. in [17, 18] to construct dynamics that (in one dimension, and in the one-fermion subspace) converges to maxima rather than minima of the potential.

2.1. Choice of boundary conditions

In the previous section, we discussed systems with detailed balance and periodic boundaries. We now discuss how the duality relation applies on finite chains with reflecting or absorbing boundaries. We note in passing that some of these relations may be generalised both to boundary-driven models and to those with a finite bias acting in the bulk [20]. However, for this work, we restrict ourselves to models without a steady-state current.

In the case of periodic boundary conditions, the derivation of our duality relations required that the rates satisfy the global constraint $\prod_i \ell_i = \prod_i r_i$, in order to guarantee detailed balance. An alternative that avoids this constraint is to use finite chains with reflecting or absorbing boundary conditions. These can be obtained by allowing zero rates in the periodic system. For a system with reflecting boundaries, we take $\ell_1 = r_N = 0$ in $W^{(1)}$. In the notation of energies, we set formally $e^{-E_{\frac{1}{2}}} = 0$: sites 1 and N are then reflecting boundaries because they are separated by an infinite barrier. This has no effect on the equilibrium steady state, which now satisfies detailed balance whatever our choice for the remaining nonzero rates. The duality transformation carries through as before, resulting in a system with $L_N = R_1 = 0$. In this system there are no transitions out of site $\frac{1}{2}$, which is therefore absorbing. The duality thus relates models with reflecting and absorbing boundaries, and as before these models share the same eigenvalues and their eigenvectors (for nonzero eigenvalues) are related through the operators S and \bar{S} . Note that for $W^{(1/2)}$, the steady state that is reached in the long-time limit has the particle fully localised on the absorbing site $\frac{1}{2}$. In this case, local detailed balance holds everywhere, but global detailed balance holds only in the trivial sense that there are no transitions taking place at all in steady state.

One can go further by distinguishing whether the absorbing site in $W^{(1/2)}$ is reached from the left (from site $\frac{3}{2}$) or from the right (from site $N - \frac{1}{2}$), and accordingly split the absorbing site into two sites $\frac{1}{2}$ and $N + \frac{1}{2}$. The duality relation to the system

$W^{(1)}$ with two reflecting boundaries then holds as before. The only difference is that, because the system now has two absorbing sites, the master operator has two zero eigenvalues. The two corresponding right eigenvectors are localised on the absorbing sites, while the elements of the left eigenvectors give the probabilities that a particle initially on a given site will end up on one or other of the absorbing sites (this will be discussed further in later sections).

Finally, one may also take an operator $W^{(1)}$ with one reflecting boundary and an absorbing site at the other boundary: this can be done by setting $e^{-E\frac{1}{2}} = 0$ and $e^{-E_N} = 0$, so that $\ell_1 = \ell_N = r_N = 0$. In the dual model of this system, $R_1 = R_N = L_N = 0$, so that the reflecting boundary at site 1 maps to an absorbing boundary at site $\frac{1}{2}$ and *vice versa* for sites N and $N - \frac{1}{2}$.

3. Propagators

We now consider the propagators of these hopping models. For convenience, we first consider periodic boundaries in the case where detailed balance holds. Generalisations to reflecting/absorbing boundaries are straightforward using the approach discussed above (Sec. 2.1). For the model $W^{(1)}$, we define the *propagator* $G_{n,m}^{(1)}(t)$ as the probability that the particle is on site n , given that it was on site m a time t earlier:

$$G_{n,m}^{(1)}(t) = \langle n | e^{W^{(1)}t} | m \rangle \quad (18)$$

Similarly, for the model $W^{(1/2)}$, we define

$$G_{n+\frac{1}{2},m+\frac{1}{2}}^{(1/2)}(t) = \langle n + \frac{1}{2} | e^{W^{(1/2)}t} | m + \frac{1}{2} \rangle \quad (19)$$

Detailed balance holds for both models so we have, bearing in mind our sign convention for energies, $G_{n,m}^{(1)}(t)e^{E_m} = G_{m,n}^{(1)}(t)e^{E_n}$ or

$$e^{-E_n} G_{n,m}^{(1)}(t) = e^{-E_m} G_{m,n}^{(1)}(t), \quad (20)$$

with a similar relation for $G^{(1/2)}$. We now appeal to the duality relation $\bar{S}W^{(1)} = W^{(1/2)}\bar{S}$ to obtain $\langle n + \frac{1}{2} | \bar{S} e^{W^{(1)}t} | m \rangle = \langle n + \frac{1}{2} | e^{W^{(1/2)}t} \bar{S} | m \rangle$. Using the explicit form of \bar{S} , we arrive at

$$e^{-E_n} G_{n,m}^{(1)}(t) - e^{-E_{n+1}} G_{n+1,m}^{(1)}(t) = \left[G_{n+\frac{1}{2},m+\frac{1}{2}}^{(1/2)}(t) - G_{n+\frac{1}{2},m-\frac{1}{2}}^{(1/2)}(t) \right] e^{-E_m}, \quad (21)$$

from which detailed balance for $W^{(1)}$ implies

$$G_{m,n}^{(1)}(t) - G_{m,n+1}^{(1)}(t) = G_{n+\frac{1}{2},m+\frac{1}{2}}^{(1/2)}(t) - G_{n+\frac{1}{2},m-\frac{1}{2}}^{(1/2)}(t). \quad (22)$$

This result generalises Eq. (5) of Ref. [10]. (We note that the latter, less general, statement is also implicit in the work of Ref. [21]; it reads in the notation there $f(q)\hat{\Gamma}_{qq'}^B(z) = \hat{\Gamma}_{qq'}^T(z)f(q')$ and can be derived by inserting Eqs. (2.15) and (2.16) into (2.19) of Ref. [21] and expanding appropriately.)

The equality (22) relates differences with respect to the initial site of propagators in the two hopping models. If the propagator for one model is known, the other can be calculated by successive application of this equation. An illustration of this relation is shown in Fig. 2. We also note that (22) is symmetric between the two master operators: any set of transition rates can be interpreted either as a model of type $W^{(1)}$ or as a model of type $W^{(1/2)}$. To reinforce this symmetry, we note that the relation $\langle n | S e^{W^{(1/2)}t} | m - \frac{1}{2} \rangle = \langle n | e^{W^{(1)}t} S | m - \frac{1}{2} \rangle$ implies that

$$e^{-E_{n-\frac{1}{2}}} G_{n-\frac{1}{2},m-\frac{1}{2}}^{(1/2)}(t) - e^{-E_{n+\frac{1}{2}}} G_{n+\frac{1}{2},m-\frac{1}{2}}^{(1/2)}(t) = \left[G_{n,m}^{(1)}(t) - G_{n,m-1}^{(1)}(t) \right] e^{-E_{m-\frac{1}{2}}} \quad (23)$$

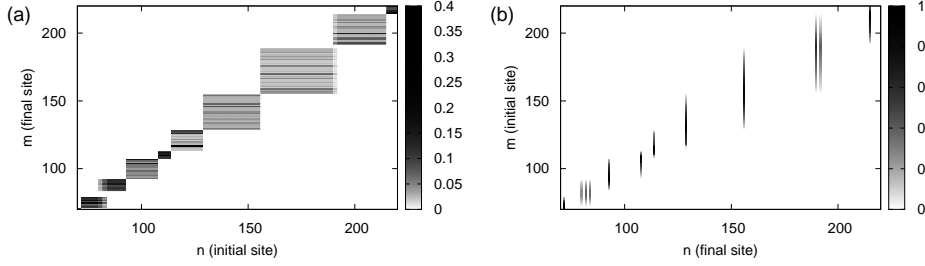


Figure 2. Plots of Green's functions that illustrate the duality relation between the propagators. The plots were generated using the effective dynamics scheme described in section 4, but (22) applies to propagation under the effective dynamics as well as to propagation with real dynamics. (Left) Propagator $G_{m,n}$, describing motion from site n to site m in a model of mixed trap-barrier type with $\mu_B = 3$ and $\mu_T = 0.5$ (see Sec. 5.1 for definitions). The 'squares' represent 'trap regions' within which the particle is locally equilibrated. The structure within the trap depends on the final site energies. These energies are randomly distributed, so that sites with low energy $-E_i$ give rise to dark 'stripes'. However, local equilibration within the trap means that the propagator depends weakly on the initial site n for all the n within a single trap. (Right) Propagator $G_{n,m}$ in the dual model of that shown on the left: note that m is now the initial site and n the final site. The probability for the final position is localised on a few deep 'trap' sites. Eq. (22) states that for given values of m and n , the gradient of the right plot in the vertical (m)-direction is equal to the gradient of the left plot in the horizontal (n)-direction.

which is the same relation as (21), but with the original model $W^{(1)}$ expressed in the form $W^{(1/2)}$ and *vice versa*.

The simple form of (22) means that we can take the disorder average. As long as the disorder is translationally invariant, e.g. if the transition state energies $\{E_{i+\frac{1}{2}}\}$ and site energies $\{E_i\}$ are taken from two (possibly different) translationally invariant distributions, the disorder-averaged propagators $\overline{G}_{n,m}(t)$ will depend only on $k = n - m$. Defining then $\Delta_k = \overline{G}_k^{(1)}(t) - \overline{G}_{-k}^{(1/2)}(t)$, the relation (22) becomes $\Delta_{-k} = \Delta_{-k-1}$. Thus, Δ_k is a constant; but $\sum_k \overline{G}_k^{(1)}(t) = 1$ and similarly for $\overline{G}_k^{(1/2)}(t)$, so $\sum_k \Delta_k = 0$ and the constant has to vanish. One concludes that $\overline{G}_k^{(1)}(t) = \overline{G}_{-k}^{(1/2)}(t)$. Re-instating the notation with separate initial and final site labels, we have

$$\overline{G}_{m,n}^{(1)}(t) = \overline{G}_{n,m}^{(1/2)}(t) = \overline{G}_{m,n}^{(1/2)}(t) \quad (24)$$

where the last equality follows from left-right symmetry. Remarkably, then, the disorder-averaged propagators of the dual models are equal on all scales of length and time. Again, this generalises our earlier statement [10] relating average propagators in pure trap and barrier models.

A similar result applies for disorder distributions which break left-right symmetry, as long as they remain translationally invariant. Take for example a model described by $W^{(1)}$ with site and barrier energies from a translationally invariant distribution, and then modify the rates according to a site-independent prescription, so that the left-going and right-going rates acquire different distributions. With periodic boundary conditions this would generally violate detailed balance, so we consider instead a long

chain with reflecting boundaries. Sufficiently far from these boundaries, translation invariance still holds and so we obtain by the same arguments as above

$$\overline{G}_{m,n}^{(1)}(t) = \overline{G}_{n,m}^{(1/2)}(t), \quad (25)$$

with both sides again depending only on the difference $k = n - m$.

4. Effective dynamics scheme

Several effective dynamics schemes have been proposed to approximate propagators for motion in random potentials. The most notable success in this area is the work of le Doussal, Monthus and Fisher [11], which we refer to as DMF. They considered the Sinai model [22], in which the r_i and ℓ_i are independently and identically distributed, so that the site energies E_i follow a random walk in real space. For long time scales in that model, DMF found a renormalisation group (RG) scheme that can be implemented analytically and gives exact results for a variety of observables.

Later, Monthus [16] applied a related scheme to the pure trap model, in which $\ell_i = r_i$ and these rates are independently and identically distributed with a power-law distribution $P(r_i) \propto r_i^{(1/\mu)-1}$. We refer to this scheme as Mon03: it can be treated analytically and its predictions are exact in the limit of large μ (our notation follows that of [10]: to arrive at the notation of [16], replace μ by $\frac{1}{\mu}$). Finally, we recently [10] introduced a modified scheme for pure trap and barrier models that respects the duality symmetry (22) but requires a computational implementation. This prescription accounts for effects that were neglected in previous schemes, and reduces to the Mon03 scheme in the limits in which that method is exact.

Here, we generalise the scheme of [10] to general disordered potentials. We arrive at a method that encompasses the DMF and Mon03 methods in the limits when they are exact, and is also consistent with the duality relation (22). We describe the application of this scheme to models parameterised in the form of $W^{(1)}$, with site energies E_i and transition state energies $E_{i+\frac{1}{2}}$. For notational convenience, we simply denote these master operators by W from now on.

4.1. Approximate propagator on a time scale Γ^{-1}

The progress of the effective dynamics is parameterised by a time scale Γ^{-1} . For a given value of Γ , the original sites and transition states of the model are combined into ‘effective traps’ and ‘effective barriers’. The procedure is illustrated in Fig. 3. Each effective trap contains at least one site; if it contains more than one site then it also contains the transition states between these sites. Similarly, each effective barrier contain at least one transition state, and also includes any sites lying between its constituent transition states. Physically, the effective traps are regions that are locally equilibrated on the time scale Γ^{-1} , while effective barrier regions are those from which the particle is likely to be absorbed into one of the adjacent effective traps.

To obtain the approximate propagator on a given time scale, we assign to each effective trap a label α and a ket $|P_\alpha\rangle$ so that for sites i within trap α ,

$$\langle i|P_\alpha\rangle = e^{E_i - F_\alpha} \quad (26)$$

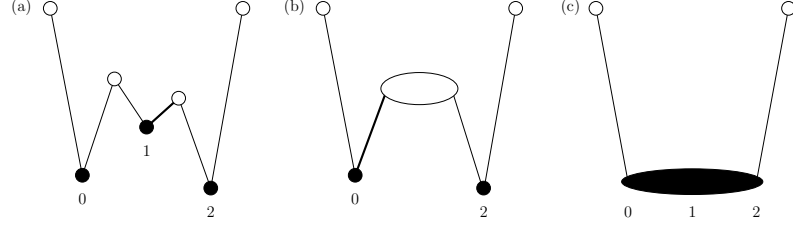


Figure 3. Illustration of the RG scheme introduced in this paper, discussed in the main text and in Appendix A. As in Fig. 1, sites are shown with closed circles and transition states with open circles. However, we now introduce effective trap regions, represented by filled ovals, and effective barrier regions, represented by open ovals. (a) Energy landscape associated with the bare master operator (36). The fastest rate r_1 is associated with the energy difference $E_1 + E_{\frac{3}{2}}$: the link associated with this rate is emphasised by a bold line. (b) Energy landscape associated with the master operator of (42) and the approximate propagator of (41). The transition states $\frac{1}{2}$ and $\frac{3}{2}$ and site 1 have been incorporated into a composite transition state, which we refer to as an effective barrier region. Within the effective dynamics presented here, a particle initially on site 1 relaxes either to site 0 or site 2, with probabilities given by the elements of the state vectors $\langle Q|$, constructed as in (30). The link associated with the largest rate in the renormalised master operator is again emphasised. (c) Energy landscape associated with the approximate propagator of (43). The two effective traps on sites 0 and 2 have been combined into a single effective trap. Within the effective dynamics, particles initially on any of these sites relax to an equilibrium distribution over sites 0, 1, 2.

is the Boltzmann-distributed probability, assuming local equilibrium within the trap. Here,

$$e^{F_\alpha} = \sum_{i \in \alpha} e^{E_i} \quad (27)$$

where the sum runs over sites in the effective trap α . We identify F_α as the free energy of the effective trap, noting that the F_α are measured downwards from an arbitrary zero, in a similar way to E_i (a large energy or free energy implies a large Gibbs weight).

Each trap is also associated with a bra state $\langle Q_\alpha|$ such that $\langle Q_\alpha|i\rangle$ is the probability that a particle initially on site i visits trap α before any other effective trap. To construct this eigenvector we consider the effective barriers $\alpha \pm \frac{1}{2}$ to the left and right of trap α . Let the left and rightmost sites in trap α be a_α and b_α . For example, the composite effective trap in Fig. 3c has $a = 0$ and $b = 2$. Clearly, for sites i within effective trap α one has $\langle Q_\alpha|i\rangle = 1$. For sites i within an effective barrier region to the left of trap α , the probability of first visiting the trap to the right, i.e. trap α , is

$$v_i^{(\alpha-\frac{1}{2})} = e^{-F_{\alpha-\frac{1}{2}}} \sum_{j=b_{\alpha-1}}^{i-1} e^{E_{j+\frac{1}{2}}} \quad (28)$$

with

$$e^{F_{\alpha-\frac{1}{2}}} = \sum_{j=b_{\alpha-1}}^{a_\alpha-1} e^{E_{j+\frac{1}{2}}}. \quad (29)$$

To prove this relation, consider the master operator for a finite system with absorbing sites at $b_{\alpha-1}$ and a_α . Then it can be verified that $\langle V_\alpha| = \langle a_\alpha| + \sum_{i=b_{\alpha-1}+1}^{a_\alpha-1} \langle i|v_i^{(\alpha-\frac{1}{2})}$

is a left zero eigenvector and that its elements give the probability of absorption on site a_α .

Combining these results, we have the probabilities for visiting trap α before any other trap:

$$\langle Q_\alpha | i \rangle = \begin{cases} v_i^{(\alpha-\frac{1}{2})}, & b_{\alpha-1} < i < a_\alpha \\ 1, & a_\alpha \leq i \leq b_\alpha \\ 1 - v_i^{(\alpha+\frac{1}{2})}, & b_\alpha < i < a_{\alpha+1} \end{cases} \quad (30)$$

As we discuss in the next section, the effective dynamics scheme rests on the assumption that motion within the effective traps is much faster than motion between them. In this case, the time evolution operator for a time Γ^{-1} simply projects the initial state onto a linear combination of equilibrium states within the effective traps:

$$\exp(W/\Gamma) \approx \mathcal{P}(\Gamma) = \sum_\alpha |P_\alpha\rangle \langle Q_\alpha|. \quad (31)$$

The approximate propagator $\mathcal{P}(\Gamma)$ depends on the set of effective traps and effective barriers that are relevant on the time scale Γ^{-1} . The effective dynamics scheme is a method of identifying these barriers. We also note that $\mathcal{P}(\Gamma)$ is a projection operator, since $\mathcal{P}(\Gamma)^2 = \mathcal{P}(\Gamma)$.

4.2. Separation of time scales

The approximation of (31) relies on a separation of time scales between intra-trap and inter-trap motion. Briefly, any master operator can be diagonalised as $W = -\sum_\lambda |\lambda\rangle \lambda \langle \lambda|$ and its propagator written as $e^{Wt} = \sum_\lambda |\lambda\rangle e^{-\lambda t} \langle \lambda|$. Time scales are (globally) well-separated if there is a time t such that all of the exponential factors are either negligibly small or close to unity. For times t with that property, the time evolution operator is well-approximated by a projection operator

$$e^{Wt} \approx \mathcal{P}_{\text{ex}}(t^{-1}) \equiv \sum_{\lambda < t^{-1}} |\lambda\rangle \langle \lambda|, \quad (32)$$

which can be written in a form similar to (31): $e^{Wt} \approx \sum_\alpha |p_\alpha\rangle \langle q_\alpha|$ where the states $|p_\alpha\rangle$ and $\langle q_\alpha|$ have non-negative elements [23]. As described above for the specific case of hopping models, the states $|p_\alpha\rangle$ indicate the regions of configuration space into which the system relaxes on these time scales and the vectors $\langle q_\alpha|$ indicate the probability of relaxing into these states.

For the renormalisation scheme, the key point is that motion on time scales longer than $t = \Gamma^{-1}$ can be well-described by a renormalised master operator $W_{\text{R,ex}}(\Gamma) = \mathcal{P}_{\text{ex}}(\Gamma) W \mathcal{P}_{\text{ex}}(\Gamma)$, since eigenmodes with $\lambda t \gg 1$ that are irrelevant at time t are also irrelevant for all longer times [more precisely, $e^{Wt} = e^{W_{\text{R,ex}}(\Gamma)t} + O(e^{-\Gamma t})$ and the error becomes small for $t \gg \Gamma^{-1}$]. In our RG scheme, we start with a set of effective trap and barrier regions for a given time scale, and then use (31) to construct the operator $\mathcal{P}(\Gamma)$ which separates fast intra-trap motion from slow motion between traps. The operator $\mathcal{P}(\Gamma)$ is an approximation to $\mathcal{P}_{\text{ex}}(\Gamma)$. The Γ -dependence of $\mathcal{P}(\Gamma)$ is obtained by constructing an approximation to the fastest eigenvectors of $W_{\text{R}}(\Gamma)$: that is, the eigenvectors with eigenvalues close to Γ . By projecting out these fast eigenvectors, we obtain an operator $\mathcal{P}(\Gamma - \delta\Gamma)$ which is an approximation to $\mathcal{P}_{\text{ex}}(\Gamma - \delta\Gamma)$. Hence, $W_{\text{R}}(\Gamma - \delta\Gamma) = \mathcal{P}(\Gamma - \delta\Gamma) W_{\text{R}}(\Gamma) \mathcal{P}(\Gamma - \delta\Gamma)$ is an approximation to $W_{\text{R,ex}}(\Gamma - \delta\Gamma)$, allowing the RG scheme to proceed iteratively.

In the next section, we present this procedure, with further discussion in Appendix A. It yields a renormalised master operator for motion on time scales longer than Γ^{-1} :

$$\begin{aligned} W_R(\Gamma) &= \sum_{\alpha} (|P_{\alpha+1}\rangle - |P_{\alpha}\rangle) (r_{\alpha} \langle Q_{\alpha}| - \ell_{\alpha+1} \langle Q_{\alpha+1}|) \\ &= \sum_{\alpha} (|P_{\alpha+1}\rangle - |P_{\alpha}\rangle) e^{-F_{\alpha} + \frac{1}{2}} (e^{-F_{\alpha}} \langle Q_{\alpha}| - e^{-F_{\alpha+1}} \langle Q_{\alpha+1}|) \end{aligned} \quad (33)$$

where the state vectors $|P_{\alpha}\rangle$ and $\langle Q_{\alpha}|$ were defined in the previous section. As required for a consistent renormalisation group flow, the operator $W_R(\Gamma)$ is of the same form as W , in that the states $|P_{\alpha}\rangle$ are arranged on a line with hopping between nearest neighbours only. [It is easily verified from the definitions that $\langle Q_{\alpha}|P_{\alpha'}\rangle = \delta_{\alpha,\alpha'}$ and $\sum_{\alpha} \langle Q_{\alpha}| = \sum_i \langle i|$, so that W_R can indeed be interpreted as a master operator.] The rates for hops to the right and left are $r_{\alpha} = e^{-F_{\alpha} - F_{\alpha+1} + \frac{1}{2}}$ and $\ell_{\alpha} = e^{-F_{\alpha} - F_{\alpha-1} + \frac{1}{2}}$, so that free energies of effective traps or barriers replace energies of bare sites and transition states, respectively.

The renormalisation scheme has two sources of error. Firstly, for typical times t , there will be eigenvalues λ of the exact master operator such that $\lambda \approx t^{-1}$, so that even the exact projection operator $\mathcal{P}_{\text{ex}}(t^{-1})$ differs from e^{Wt} . However, as discussed above, the approximation $e^{Wt} \approx e^{W_{\text{ex,R}}(\Gamma)t}$ is accurate for large Γt so while there are errors at any given time, they do not accumulate as the scheme progresses and the renormalised propagator remains close to the exact one.

The more important errors in our scheme arise from a different source: the scheme yields an operator $\mathcal{P}(\Gamma)$ that is an approximation to $\mathcal{P}_{\text{ex}}(\Gamma)$. For general hopping models, differences between $\mathcal{P}(\Gamma)$ and $\mathcal{P}_{\text{ex}}(\Gamma)$ may accumulate as the scheme proceeds, leading to large errors in the propagator. The conditions under which the operator $\mathcal{P}(\Gamma)$ represents a good approximation to $\mathcal{P}_{\text{ex}}(\Gamma)$ are discussed in Appendix A. To summarise the results given there, on long time scales (small Γ) one may identify ‘fast relevant rates’ which are associated with motion on time scales comparable to Γ^{-1} . For a consistent renormalisation flow, we require that fast relevant rates are typically much larger than all other relevant rates in their neighbourhood, except that (i) fast relevant rates r_{α} may be comparable either to ℓ_{α} or to $\ell_{\alpha+1}$, and (ii) fast relevant rates ℓ_{α} may be comparable either to r_{α} or to $r_{\alpha-1}$. (The condition of globally well-separated time scales described above is not required: it is sufficient that eigenvalues for motion in the same spatial neighbourhood should be well-separated.)

Comparing with previous schemes, the original treatment of DMF applies when all rates r_i and ℓ_i are independently distributed. That case is the Sinai model [22] and, at long times, fast rates r_{α} are typically well-separated from *both* ℓ_{α} and $\ell_{\alpha+1}$. (Of course, in a large enough system there will always be regions where $r_{\alpha} \approx \ell_{\alpha}$. However, as discussed by DMF [11], the condition that typical rates be well-separated is sufficient for a consistent RG scheme and allows many quantities to be derived exactly from the effective dynamics.) Turning to other hopping models, the pure trap model has transition state energies $E_{i+\frac{1}{2}} = 0$ for all i , while the site energies E_i are independently distributed. In this case, rates ℓ_{α} and r_{α} are of the same order and the scheme of DMF must be modified: two possible modifications that are specific to pure traps/pure barriers are given in Refs. [16, 10]. The scheme described here generalises the methods of [16] and [10] since it is not restricted to pure trap and barrier models. It improves on the method of DMF in that it relaxes the assumption that all relevant fast rates in a neighbourhood are well-separated, allowing that fast right-moving rates

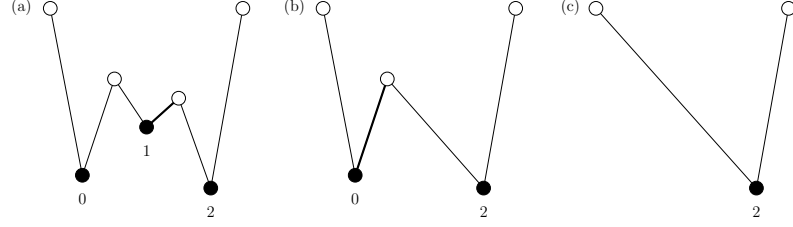


Figure 4. Illustration of the RG scheme of DMF, discussed in the main text. (a) Energy landscape associated with the bare master operator (36). The fastest rate r_1 is associated with the energy difference $E_1 + E_{\frac{3}{2}}$: the link associated with this rate is emphasised in bold. (b) Energy landscape associated with the master operator of (38) and the approximate propagator of (39). Within the effective dynamics scheme of DMF, the fast motion on these time scales involves a particle initially on site 1 relaxing onto site 2, with probability unity. The link associated with the largest rate of the resulting master operator is again emphasised. (c) Energy landscape associated with the approximate propagator of (40). Within the effective dynamics of DMF, particles initially on sites 0, 1 or 2 will relax onto site 2.

may be comparable to one of their neighbouring left-moving rates, and *vice versa*. Further, as we approach the limit of well-separated local rates, the scheme presented here captures non-perturbative corrections that are not present in DMF, as we discuss in section 5. We will see that the scheme is natural and quite simple to implement numerically.

4.3. Renormalisation of the effective master operator

So far, we have explained how the effective traps and barriers are related to propagation in these systems. We now explain how the set of traps and barriers on a given time scale are obtained from those on some smaller time scale. We give the method here, deferring some further details and justifications to Appendix A. Initially each effective trap contains a single site i , and each effective barrier a single transition site $i + \frac{1}{2}$. Each stage of our effective dynamics begins by calculating an approximate eigenvalue of $W_R(\Gamma)$ associated with fast motion, as follows. For each trap α , we calculate a rate for motion associated with the rate r_α , i.e. with leaving the trap to the right:

$$\rho_\alpha = \frac{1}{2}(r_\alpha + \ell_\alpha + \ell_{\alpha+1}) + \frac{1}{2}\sqrt{r_\alpha^2 + 2r_\alpha(\ell_\alpha + \ell_{\alpha+1}) + (\ell_\alpha - \ell_{\alpha+1})^2}. \quad (34)$$

and similarly for motion associated with the rate l_α :

$$\lambda_\alpha = \frac{1}{2}(\ell_\alpha + r_\alpha + r_{\alpha-1}) + \frac{1}{2}\sqrt{\ell_\alpha^2 + 2\ell_\alpha(r_\alpha + r_{\alpha-1}) + (r_\alpha - r_{\alpha-1})^2}. \quad (35)$$

Notice that ρ_α is symmetric in ℓ_α and $\ell_{\alpha+1}$. In a (renormalised) landscape similar to that for pure traps, ℓ_α would be comparable to r_α and so $\rho_\alpha \approx r_\alpha + \ell_\alpha$ if the other rate ($\ell_{\alpha+1}$) is small. Conversely, in a landscape resembling pure barriers, one would have $\ell_{\alpha+1}$ of the same order as r_α and so to leading order $\rho_\alpha \approx r_\alpha + \ell_{\alpha+1}$. The expressions (34,35) cover both of these limits but extend them to general landscapes.

Having calculated the ρ_α and λ_α , we select the largest of these eigenvalues across all traps, and update $\Gamma = t^{-1}$ to this largest eigenvalue. Supposing that the largest eigenvalue is ρ_α associated with motion to the right from trap α , we now want to

remove trap α and the barrier region $\alpha + \frac{1}{2}$ to its right. We make a case distinction, depending on whether the local landscape is nearer to the pure trap or the pure barrier case, as in the discussion of the rate-dependence of ρ_α above. If $\ell_{\alpha+1} > \ell_\alpha$ we merge α and $\alpha + \frac{1}{2}$ to the right, i.e. we combine traps α and $\alpha + 1$. The condition on the rates means physically that there is a higher barrier to the left of trap α than to the left of $\alpha + 1$ (see also Fig. 3), so that it makes sense to combine these traps. Conversely, if $\ell_{\alpha+1} < \ell_\alpha$, we merge α and $\alpha + \frac{1}{2}$ to the left, which amounts to combining barrier regions $\alpha \pm \frac{1}{2}$. This is the case where the barrier to the left of trap α , leading up to barrier $\alpha - \frac{1}{2}$, is low and so we should incorporate the trap-barrier pair $\alpha, \alpha + \frac{1}{2}$ into barrier $\alpha - \frac{1}{2}$. For the case where the largest eigenvalue is λ_α , associated with motion to the left, the rules are similar, in accordance with left-right symmetry: if $r_{\alpha-1} > r_\alpha$ we combine traps $\alpha - 1$ and α (we merge $\alpha - \frac{1}{2}$ and α to the left); otherwise we combine barrier regions $\alpha \pm \frac{1}{2}$ (merge to the right).

Having combined two traps or barriers and the barrier/trap region between them, we finally recalculate the relevant free energy, and the hopping rates r_α and ℓ_α and associated eigenvalues ρ_α and λ_α that are affected by the change. From here on the process is iterated, i.e. we find the largest rate among the $\{\rho_\alpha, \lambda_\alpha\}$, update Γ , and merge the appropriate traps or barriers. After each update of Γ , the propagator is $G_{n,m} = \langle n | \mathcal{P}(\Gamma) | m \rangle$ from Eq. (31).

The scheme of DMF can be expressed as a limit of the RG scheme above, where all energies are taken to be widely separated locally. This means that (a) the free energy of each effective trap or barrier is approximated as being dominated by the *largest* energy, e.g. $F_\alpha = \max_{i \in \alpha} E_i$, and (b) the local rates are also taken as widely separated, so that one approximates $\rho_\alpha = r_\alpha$ and $\lambda_\alpha = \ell_\alpha$. Under these conditions, all elements $\langle i | P_\alpha \rangle$ are negligible except for the site in the trap with the largest E_i , and all elements $\langle Q_\alpha | j \rangle$ are either 1 or zero according to whether site j is nearer to effective trap α than the transition state (in the same effective barrier region as j) with the largest $E_{i+\frac{1}{2}}$. The propagator, given by the matrix elements of the projection operator $\mathcal{P}(\Gamma)$, then takes only the values 0 or 1 and the effective dynamics can be regarded as deterministic, or as a ‘zero-temperature’ approximation.

We now illustrate both our current scheme and that of DMF using the example landscape shown in Fig. 3, concentrating on sites 0, 1, 2 of a long chain. The bare master operator is therefore

$$\begin{aligned} W &= \dots + (|0\rangle - |1\rangle)(\ell_1\langle 1| - r_0\langle 0|) + (|1\rangle - |2\rangle)(\ell_2\langle 2| - r_1\langle 1|) + \dots \\ &= \dots + (|0\rangle - |1\rangle)e^{-E_{\frac{1}{2}}}(\langle 1| - e^{-E_0}\langle 0|) \\ &\quad + (|1\rangle - |2\rangle)e^{-E_{\frac{3}{2}}}(\langle 2| - e^{-E_1}\langle 1|) + \dots \end{aligned} \quad (36)$$

where the \dots indicate the remaining terms in the master operator, including those for hopping into and out of this segment of the chain. Consistent with Fig. 3a, we choose the rates to lie in three well-separated sectors:

$$r_1, \ell_1 \gg r_0, \ell_2 \gg \ell_0, r_2. \quad (37)$$

For concreteness we also take $r_1 > \ell_1$ (i.e. $E_{\frac{1}{2}} > E_{\frac{3}{2}}$), $\ell_2 > r_0$ and $E_2 > E_0$.

We start by illustrating the simpler DMF scheme, as shown in Fig. 4. Beginning with Fig. 4a, the largest rate is $\rho_1 \equiv r_1$ so we set $\Gamma = r_1$ and remove site 1 and transition state $\frac{3}{2}$, as illustrated in Fig. 4b. This creates an effective trap containing sites 1 and 2. (Equivalently we could think of an effective barrier region containing sites $\frac{1}{2}$ and $\frac{3}{2}$ and an effective trap containing only site 2; the difference is immaterial in

the DMF scheme because either way site 1 is assigned zero probability of occupation.) The projection operator at this stage is

$$\mathcal{P} = \cdots + |0\rangle\langle 0| + |2\rangle(\langle 1| + \langle 2|) + \cdots \quad (38)$$

where we show only the elements relevant for this part of the chain. We can also construct the renormalised master operator for time scales longer than $\Gamma^{-1} = 1/r_1$:

$$W_R = \mathcal{P}W\mathcal{P} = \cdots + (|0\rangle - |2\rangle)e^{-E\frac{1}{2}}(e^{-E_2}\langle 2| - e^{-E_0}\langle 0|) + \cdots \quad (39)$$

At the next stage of the procedure, the largest rate is $r'_0 \equiv e^{-E_0-E\frac{1}{2}}$ (because $E_2 > E_0$), so we set $\Gamma = r'_0$ and remove site 0 and transition state $\frac{1}{2}$. The projection operator on time scales longer than Γ^{-1} is therefore

$$\mathcal{P}' = \cdots + |2\rangle(\langle 0| + \langle 1| + \langle 2|) + \cdots \quad (40)$$

That is, particles initially on sites 0, 1, 2 all relax onto site 2, on this time scale. The renormalised master operator at this second stage, $W'_R = \mathcal{P}'W_R\mathcal{P}' = \mathcal{P}'W\mathcal{P}'$, has no terms for mixing sites within the set $\{0, 1, 2\}$, although it does contain hopping terms between site 2 and sites -1 and 3 .

We next examine how our own RG scheme as described above proceeds for the energy landscape of (36) and Figs. 3 and 4. From the assumptions (37), the largest of the ρ and λ -rates at the initial stage will be ρ_1 , which is associated with rate r_1 , i.e. with motion out of trap 1 and across barrier $\frac{3}{2}$. (To leading order in the largest rates r_1 and ℓ_1 , $\rho_1 = \lambda_1 = r_1 + \ell_1$; but the correction from ℓ_2 can then be shown to make $\rho_1 > \lambda_1$.) We thus set $\Gamma = \rho_1$. From (37), we have $\ell_2 < \ell_1$, so we combine transition states $\frac{1}{2}$ and $\frac{3}{2}$ into a single effective barrier: trap 1 and barrier $\frac{3}{2}$, which we want to remove, are “nearer” barrier $\frac{1}{2}$ than trap 2. We use (30) to construct vectors $\langle Q_0| = \langle 0| + e^{\frac{E_1}{2}-F}\langle 1|$ and $\langle Q_2| = \langle 2| + e^{\frac{E_3}{2}-F}\langle 1|$, where $e^F = e^{\frac{E_1}{2}} + e^{\frac{E_3}{2}}$ so that F (more systematically one could write $F_{\frac{1}{2}\frac{3}{2}}$) is the free energy of the effective barrier region, as in Eq. (29). The vectors $\langle Q_0|, \langle Q_2|$ are associated with relaxation from this region onto sites 0 and 2. The result is an operator that projects onto modes with eigenvalues smaller than $\Gamma = \rho_1$:

$$\mathcal{P} = \cdots + |0\rangle\langle Q_0| + |2\rangle\langle Q_2| + \cdots \quad (41)$$

The renormalised master operator for motion on time scales longer than $\Gamma^{-1} = 1/\rho_1$ is then

$$W_R = \mathcal{P}W\mathcal{P} = \cdots + (|0\rangle - |2\rangle)e^{-F}(e^{-E_2}\langle Q_2| - e^{-E_0}\langle Q_0|) + \cdots \quad (42)$$

For the next stage of the effective dynamics, the largest hopping rates are $r'_0 = e^{-F-E_0}$, for hopping from trap 0 to the right, and $\ell'_2 = e^{-F-E_2}$, for going from trap 2 to the left. Because $E_2 > E_0$, the former will be larger than the latter, and the remaining rates $\ell'_0 = \ell_0$ and $r'_2 = r_2$ are much smaller by our assumption (37). Correspondingly, when we calculate the approximate eigenvalues ρ'_α and λ'_α derived from W_R , the largest one will be ρ'_0 , which is associated with r'_0 . From the assumptions (37), we have $\ell'_0 \ll \ell'_2$, so we combine sites 0 and 2 with their intervening barrier region, forming a new effective trap. Constructing the eigenstate $|P_{012}\rangle$ for this trap in accordance with (26) gives the projection operator for motion on time scales longer than $1/\rho'_0$:

$$\begin{aligned} \mathcal{P}' &= \cdots + |P_{012}\rangle(\langle Q_0| + \langle Q_2|) + \cdots \\ &= \cdots + |P_{012}\rangle(\langle 0| + \langle 1| + \langle 2|) + \cdots \end{aligned} \quad (43)$$

Comparing with the DMF scheme, we note that our prescriptions locate the second step of the RG procedure at a larger time (smaller Γ) because the effective barrier region bounded by sites $\frac{1}{2}$ and $\frac{3}{2}$ has a free energy $F > E_{\frac{1}{2}}$. This reflects the fact that a barrier region takes longer to traverse if it contains several barrier sites with comparable energies. Similarly, after the second step our procedure keeps tracks of the finite occupation probabilities of sites 0 and 1, which arise from equilibration in the effective trap spanning sites 0, 1 and 2.

4.4. Renormalisation and duality

To conclude this section, we discuss duality relations for the effective dynamics, restoring superscripts to distinguish between $W^{(1)}$ and $W^{(1/2)}$. If we renormalise an operator $W^{(1)} = S\bar{S}$ according to our scheme, we arrive at a renormalised model that can be written in the form $W_R^{(1)} = S_R\bar{S}_R$. The operators S_R and \bar{S}_R have the same form as S and \bar{S} , except that sites i are replaced by effective traps α , transition states by effective barriers, and energies by free energies. An important property of our RG procedure is that if we apply it to the dual master operator $W^{(1/2)} = \bar{S}S$, we find that this renormalises precisely to $W_R^{(1/2)} = \bar{S}_R S_R$. Thus, in addition to the basic requirement that $W_R(\Gamma)$ takes the same form as W , our scheme also obeys the general duality relation under landscape inversion. This is of course desirable, as renormalisation schemes should respect all symmetries of the models of interest.

In the illustrations of Figs. 3 and 4, the duality property follows for both the new scheme and that of DMF, because acting on these illustrations with the inversion operation of Fig. 1 leads to the same renormalisation flows that would be obtained by starting with the model dual to (36). For example, combining two traps in a given model results in two barriers being combined in the dual model and *vice versa*.

Mathematically, the duality can be shown as follows. At each state of the RG flow we have effective trap regions α in $W_R^{(1)}$ and barrier regions $\alpha + \frac{1}{2}$; in $W_R^{(1/2)}$ the regions α with integer index are effective barriers, with effective traps in the regions $\alpha + \frac{1}{2}$. The associated free energies F_α and $F_{\alpha+\frac{1}{2}}$ are the same in both cases. The dual model $W_R^{(1/2)}$, written in trap model notation, then has hopping rates $r_{\alpha-\frac{1}{2}} = \ell_\alpha$ and $\ell_{\alpha+\frac{1}{2}} = r_\alpha$, and one easily checks that analogous relations hold for the approximate eigenvalues of the master operator, i.e. $\rho_{\alpha-\frac{1}{2}} = \lambda_\alpha$ and $\lambda_{\alpha+\frac{1}{2}} = \rho_\alpha$. Thus at each renormalisation step we will remove the same trap-barrier pair in both models, and it can be verified that also the decision whether to merge to the left or right is the same. This implies that the entire RG flow is identical for $W^{(1)}$ and $W^{(1/2)}$.

A brief comment is in order on the construction of S_R and \bar{S}_R . From $W_R^{(1)} = \mathcal{P}^{(1)}W^{(1)}\mathcal{P}^{(1)}$ and $W^{(1)} = S\bar{S}$ one might naively identify $S_R = \mathcal{P}^{(1)}S$, $\bar{S}_R = \bar{S}\mathcal{P}^{(1)}$; but this choice does not satisfy the duality requirement that $W_R^{(1/2)} = \bar{S}_R S_R$. A little thought shows that one requires instead $S_R = \mathcal{P}^{(1)}S\mathcal{P}^{(1/2)}$ and $\bar{S}_R = \mathcal{P}^{(1/2)}\bar{S}\mathcal{P}^{(1)}$. Here $\mathcal{P}^{(1/2)} = \sum_\alpha |P_{\alpha+\frac{1}{2}}\rangle\langle Q_{\alpha+\frac{1}{2}}|$ is the projector onto the effective traps of the dual model, with $|P_{\alpha+\frac{1}{2}}\rangle$ and $\langle Q_{\alpha+\frac{1}{2}}|$ constructed in the obvious manner using the duals of (26) and (30). The operators S_R and \bar{S}_R defined in this way are indeed the effective trap and barrier analogues of (7–10), and the desired dual expressions $W_R^{(1)} = S_R\bar{S}_R$ and $W_R^{(1/2)} = \bar{S}_R S_R$ therefore hold. We note finally that not only the master operators but also the propagators produced by our RG scheme obey the required duality: the propagators are the matrix elements of the projectors $\mathcal{P}^{(1)}$ and $\mathcal{P}^{(1/2)}$, and one verifies

by direct calculation that $\langle m | \mathcal{P}^{(1)}(|n\rangle - |n+1\rangle) = \langle n + \frac{1}{2} | \mathcal{P}^{(1/2)}(|m + \frac{1}{2}\rangle - |m - \frac{1}{2}\rangle)$ in accordance with the general duality relation (22).

5. Specific disorder distributions

5.1. Mixed trap-barrier models

The renormalisation scheme that we have discussed can be implemented computationally without undue difficulty. It allows rapid estimation of propagators in these hopping models, both for fixed disorder and for disorder-averaged properties. We first consider a model obtained by mixing the pure trap and barrier models defined above. In the pure trap model, the transition state energies are $E_{i+\frac{1}{2}} = 0$, while site energies are chosen from an exponential distribution with a mean of μ ; that is, $P(E_i) = (1/\mu)e^{-E_i/\mu}$ with $E_i > 0$. In terms of rates, this implies $\ell_i = r_i = w_i$ with $P(w_i) = (1/\mu)w_i^{(1/\mu)-1}$ for $0 < w_i < 1$. Similarly, pure barrier models have $E_i = 0$ for all sites, and transition state energies are exponentially distributed: that is, $L_i = R_i = w_i$ with the same distribution $P(w_i)$.

We mix these models by taking both site and transition state energies to be exponentially distributed with means μ_T and μ_B respectively. The dynamical scaling of these models therefore depends on the parameters μ_B and μ_T . For the pure barrier model ($\mu_T \rightarrow 0$), sites have half-integer indices and moving a distance r typically requires the crossing of a barrier i whose hopping rate is $w_i \sim r^{-\mu_B}$. The rate for actually crossing this barrier is suppressed because the particle is delocalised in an effective trap whose width is of order r . In the language of the effective dynamics, the landscape consists of wide effective traps separated by isolated transition states, and each site $i + \frac{1}{2}$ within the trap contributes to $e^{F_{\alpha+\frac{1}{2}}} = 1$ to $e^{F_{\alpha+\frac{1}{2}}}$. The result is that the time taken to move a distance r is $\tau(r) \sim e^{F_{\alpha+\frac{1}{2}} + E_i} \sim r/w_i \sim r^{1+\mu}$. In the pure trap model, the typical time for escaping from sites with large E_i is $1/w_i \sim e^{E_i}$, but the barrier regions on this time scale are typically of width r and their free energies therefore also scale as $e^{F_{\alpha+\frac{1}{2}}} \sim r$, reflecting the probability of reabsorption in the original trap before arriving at a new one [10]. Thus, the typical relevant time scale is again $\tau(r) \sim r^{1+\mu}$.

We define the dynamical exponent z through the relation $\tau \sim r^z$, and identify

$$z = 1 + \mu_B, \quad \mu_B > 1, \mu_T \rightarrow 0 \quad (44)$$

with an analogous relation if $\mu_T > 1$ and $\mu_B \rightarrow 0$.

In the mixed model, the crucial case distinctions are then whether the μ_B and μ_T are larger or smaller than unity. For example, if $\mu_T < 1$, the average value of e^{E_i} is finite, and the free energies of relevant trap regions scale as $e^{F_i} \sim r$. On the other hand, if $\mu_T > 1$, the site-averaged e^{E_i} is no longer finite, and the sum in (27) is dominated by the largest site within the effective trap. In this case $e^{F_i} \sim r^{\mu_T}$. A similar argument applies for μ_B . Combining these results, we arrive at the dynamic exponent for the mixed model

$$z = \max(1, \mu_B) + \max(1, \mu_T) \quad (45)$$

which reduces to the pure trap case if $\mu_B = 0$ and the pure barrier case if $\mu_T = 0$. Fig. 5 shows numerical results that are consistent with (45). Thus, the effective dynamics provide a natural framework in which to derive this kind of scaling result, although the above predictions for the dynamical exponent could presumably be obtained by other

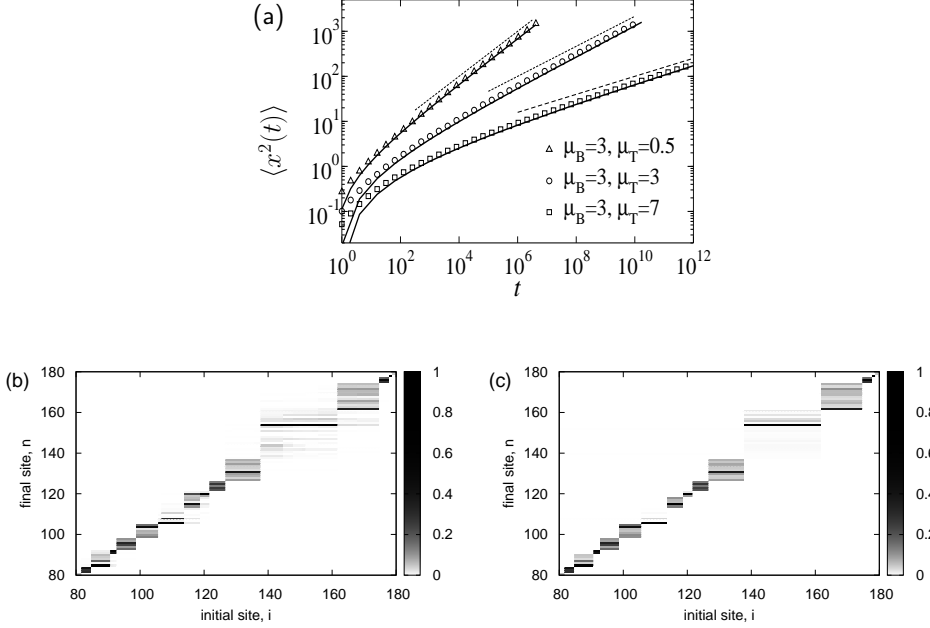


Figure 5. (a) Mean square displacement, showing real dynamics (symbols), effective dynamics (solid lines) and power law predictions of (45) (dashed lines). The DMF scheme (not shown) also gives the correct scaling as long as $\mu_B, \mu_T > 1$ but gives the wrong exponent for the case where $\mu_T = 0.5$. (b,c) Propagators for real dynamics (b) and effective dynamics (c) for the case $\mu_B = 10$ and $\mu_T = 1$. The time is $t = 2^{29}$: the propagator for the real dynamics is obtained by simulating its dual model and using (22), since models with large μ_T can be simulated much more efficiently than those with large μ_B . Since μ_B is large, nearby rates are well-separated and the effective dynamics gives a good approximation to the propagator even for fixed disorder. However, there are deviations in some neighbourhoods which are associated with the presence of eigenvalues of the same order as $1/t$, as discussed in the text.

means. We also note that the renormalisation arguments of DMF give $z = \mu_B + \mu_T$ which is the correct result when both μ_B and μ_T are greater than unity. This is consistent with our assertion above that if $\mu_B, \mu_T > 1$ the free energies of effective traps and barriers are typically dominated by single sites, and this is precisely the limit in which the scheme of DMF is valid without approximation.

In Fig. 5(b,c), we show example propagators obtained using real and effective dynamics for the case $\mu_B = 10$, $\mu_T = 1$. For these parameters, time scales in a given neighbourhood are sufficiently well-separated that the effective dynamics gives a good approximation to the propagator. In this case, it appears that the largest deviations between real and effective dynamics come from neighbourhoods in which there is an eigenvalue of W of the order of $1/t$. In the discussion of Sec. 4.2, we noted that such deviations are expected even when our scheme gives $P(\Gamma)$ exactly equal to $P_{\text{ex}}(\Gamma)$, and that the specific deviations seen at any time t should decay as time increases, so that the exact and approximate propagators remain close. Our results are consistent with this expectation. For example, comparing Figs. 5b and 5c, the effective

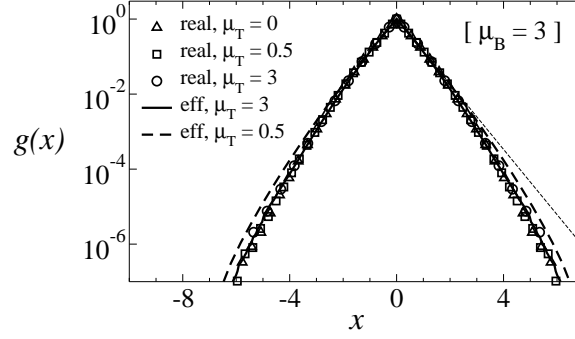


Figure 6. We show estimates of the function $g(x)$ obtained by evaluating $\overline{G}_k(t)$ for times t within the scaling regime. Results are displayed for both real and effective dynamics, with $\mu_B = 3$. Symbols show results for real dynamics with $\mu_T = 0$ (triangles), $\mu_T = 0.5$ (squares) and $\mu_T = 3$ (circles). The times are chosen to lie in the scaling regime and vary from 2^{12} to 2^{24} , according to the model: we note that while the functions $g(x)$ are similar in all cases, the values and scalings of the mean square displacements are different, according to (45). The solid line shows the result for the effective dynamics and $\mu_T = \mu_B = 3$, while the heavy dashed line shows effective dynamics for $\mu_B = 3$, $\mu_T = 0.5$. The light dashed line is a simple exponential distribution. The scheme of DMF (not shown) gives reasonable agreement for $\mu_T = \mu_B = 3$, but this agreement breaks down as μ_T (or μ_B) is reduced.

dynamics indicates that sites in the vicinity of site 110 are separated into three traps, containing sites 106-113, 114-118, and 119-121: the effective barrier regions are simply single transition states. However, the real dynamics reveals that initial sites 114 – 118 propagate both within that effective trap, and into the adjacent traps. On time scales much shorter than t , one would expect localisation within this trap; on longer time scales the trap will either merge with an adjacent trap, or become incorporated into an effective barrier region. We conclude that we have measured the propagator during this crossover, the details of which are not captured by the effective dynamics.

Moving to disorder-averaged properties, numerical results indicate that the long-time behaviour in these systems is associated with a scaling form of the diffusion front, as expected. That is (with k the distance between initial and final site as before),

$$\overline{G}_k(t) \approx \sigma^{-1} g(k/\sigma). \quad (46)$$

where the function $g(x)$ is independent of the time t and we use $\sigma = \sigma(t) = 1/\overline{G}_0(t)$ as an estimate of the length scale associated with motion on a time scale t , ensuring that $g(0) = 1$. Our numerical results then indicate that the shape of the diffusion front $g(x)$ depends quite strongly on $\max(\mu_B, \mu_T)$ and much more weakly on $\min(\mu_B, \mu_T)$. As in Ref. [10], the effective dynamics give good agreement with the real dynamics when either μ_B or μ_T is large, with deviations at smaller μ that arise because time scales associated with hopping rates in the same neighbourhood are not well-separated. We show some illustrative results in Fig. 6: the fit for the effective dynamics with $\mu_B = \mu_T = 3$ is strikingly good. However, reducing the value of μ_T further has an effect on the diffusion front for the effective dynamics, while no effect is discernable for the real dynamics. This reduces the quality of the fit in this case.

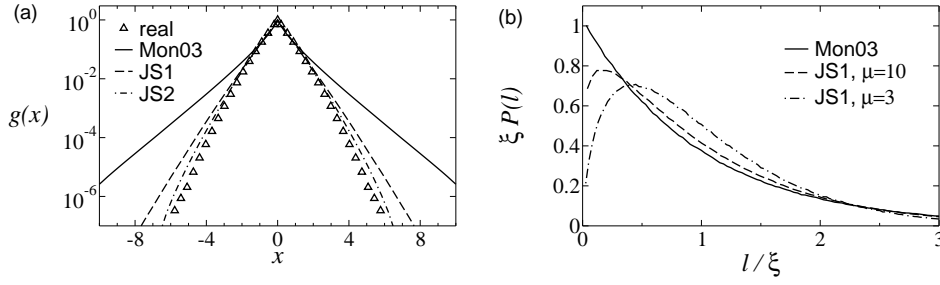


Figure 7. (a) Scaling form for the disorder-averaged diffusion front for the pure trap model with $\mu_T = 3$, $\mu_B = 0$. We show the results for real dynamics and various approximations to this function, obtained by simulations of effective dynamics schemes. All results are taken from the scaling regime, with in particular $t = 2^{17}$ for the real dynamics. We show the Mon03 scheme of Ref. [16], which yields (48); the scheme of [10] (labelled JS1); and the scheme discussed in this article (labelled JS2). (b) Distribution of barrier widths $P(l)$ in the effective dynamics, scaled by its mean ξ . We show results for the effective dynamics scheme of Mon03 in which $P(l)$ is a simple exponential, and two distributions obtained with the scheme JS1.

We also find that numerical implementation of the DMF procedure yields reasonable agreement with mean-square displacement and the diffusion front for the case $\mu_B = \mu_T = 3$. However, this agreement breaks down as μ_T is reduced: for $\mu_T < 1$, the DMF scheme yields the wrong dynamical exponent, as discussed above. Thus, the main advantage of the scheme presented here is that it captures the crossover as μ_T gets small [see Eq. (45)]; in this case, it also gives more accurate results for the propagators at fixed disorder (not shown).

Finally, we note that when calculating propagators, we expect the various schemes (DMF, Mon03, that of [10], and the one presented here) to be equivalent in the limit of large μ , at least at the level of the diffusion front. However, the approach to that limit is non-trivial and involves effects that are non-perturbative in μ : the scheme presented here captures some of these effects, which results in improved fits to the diffusion front. In the next section, we illustrate this in the case of the pure trap model. Of course, because of duality, an essentially identical discussion can be given for the pure barrier case.

5.2. Comparison of RG schemes in the pure trap models

We recall that the pure trap model is the case $\mu_B \rightarrow 0$; we then write $\mu_T = \mu$. Applying the DMF method directly to the pure trap model results in a dynamical exponent $z = \mu$. As noted in [16], this result is incorrect: the route taken by Monthus was simply to introduce a factor of the root mean square displacement when converting the rate Γ to a time t . With this change, the dynamical scaling given by the Mon03 scheme [16] is correct.

In Fig. 7, we compare the effective dynamics scheme set out in this article with that of [10] and with Mon03 [16]. The differences are quite striking, as we now discuss. In the schemes of [10] and [16], all effective trap regions are single sites, and the RG scheme relates the propagator to the distribution $P(l)$ of the widths l of effective barrier regions. [We normalise $P(l)$ to $\int_0^\infty dl l P(l) = 1$, such that the probability for a

randomly chosen transition state to be in a barrier region of width l is $lP(l)$. Results for $P(l)$ from our current RG scheme are not given here because even for a pure trap model the RG flow eventually leads to a mixture of effective traps and effective barriers which cannot be characterised by a single distribution $P(l)$.] If a given barrier region is delimited by sites b and $b+l$, then the propagator is $G_{n,m} = \delta_{n,b} \frac{b+l-m}{l} + \delta_{n,b+l} \frac{m-b}{l}$ for $b \leq m \leq b+l$. Averaging over all initial sites m at fixed $k = n - m$ on a long chain with the relevant distribution of barrier widths, we arrive at the disorder-averaged diffusion front,

$$\overline{G_k} = \int_{|k|}^{\infty} dl \frac{l - |k|}{l} P(l) \quad (47)$$

where we have assumed that t is large, so that $P(l)$ is smooth, and we may convert sums over l to integrals. Within the Mon03 scheme, the distances l are all independently and identically distributed with an exponential form $P(l) = \xi^{-2} e^{-l/\xi}$. This leads to an estimate for the diffusion front in the limit of large μ :

$$\overline{G_k} \approx \xi^{-1} e^{-k/\xi} \int_0^{\infty} dy \frac{y}{y + k/\xi} e^{-y} \quad (48)$$

so that the diffusion front is a scaling function of $x = k/\sigma$ for large times, with $\sigma = \xi$. The assumption of Ref. [16] is that, while working at large finite μ does affect $P(l)$, these changes lead to perturbative corrections to the diffusion front.

However, Fig. 7 shows that the tail of the diffusion front is rather different from the prediction (48) of Ref. [16], at least for $\mu = 3$. The effective dynamics scheme discussed in this paper gives more accurate predictions for this tail. In fact, the convergence of the tail of the diffusion front to its large- μ prediction is quite slow. Instead of plotting the diffusion front data directly, we show barrier width distributions $P(l)$ for the effective dynamics schemes of Refs. [16] and [10]. (The distribution $P(l)$ is obtained directly from the effective dynamics: in fact this was the route by which $\overline{G_k}$ was evaluated in Figs. 6 and 7(a).) If we define the mean barrier width to be ξ , then we find that $P(l)$ converges to the simple exponential distribution only if we take $\mu \rightarrow \infty$ at a fixed value of the scaling variable l/ξ . For smaller l there are corrections to this distribution that cannot be accounted for by treating $1/\mu$ perturbatively. Indeed, our numerical results are most consistent with the tail of the diffusion front scaling as

$$\log \overline{G_k} \sim -|k|^{1+\alpha} \quad (49)$$

where $\alpha > 0$ is a power that vanishes as $\mu \rightarrow \infty$. In this case it is clear that the limits of large μ and large k do not commute and hence that working perturbatively in $1/\mu$ is likely to fail when considering the large- k limit of $\overline{G_k}$. We have not found an analytical treatment which can determine the resulting exponent α , neither exactly nor for our effective dynamics. However, the numerical evidence of Fig. 7 is that our scheme does capture the non-perturbative effects which lead to slow convergence of the diffusion front to the large μ limit.

6. Outlook

In this article, we have derived duality relations that connect pairs of hopping models linked by an inversion of their energy landscape. The simplest case is that of models with equilibrium steady states and periodic boundary conditions, but we were able also to link models with absorbing and reflecting boundary conditions. Somewhat surprisingly, certain periodic systems (pure trap and barrier models with a bias) in

which the steady state has a finite current can be analysed similarly [20]. All duality relations are initially expressed in terms of the relevant master operators, but we showed that one can then also construct the propagator of each model from its dual. It follows further that the disorder-averaged propagators in each pair of models are equal on all finite time and length scales.

We have also introduced an effective dynamics scheme for these hopping models. It incorporates both the scheme of Ref. [10] and that of DMF, allowing a broad class of models to be treated in a unified fashion. For a range of “mixed trap-barrier models”, including the pure barrier and trap cases, we have also shown that our scheme captures non-perturbative corrections to the schemes of DMF and Mon03.

Our results also identify a few questions: can explicit expressions for the disorder-averaged diffusion fronts be derived for the mixed model or for the pure trap/barrier cases, either exactly or at least within the effective dynamics? It appears that the diffusion front in the mixed model depends only on the larger of μ_B and μ_T : can this be established? More speculatively, one might ask if the methods used here can be generalised in order to identify effective trap and barrier regions for higher-dimensional systems. We leave these issues for future work.

Acknowledgments

We thank Jean-Philippe Bouchaud, Jeppe Dyre, Jorge Kurchan, Peter Mayer and Cécile Monthus for helpful discussions.

Appendix A. Effective dynamics

In this appendix we give some details of the renormalisation scheme that underlies our effective dynamics. The scheme gives a good description of the dynamics of the model in the limit in which rates in the same neighbourhood are sufficiently well-separated. We first derive the version of the RG procedure that is most natural from a formal point of view, but then argue in favour of the more physically-motivated scheme described in the text on the grounds that both agree in the relevant limit where time scales are locally well-separated.

Appendix A.1. Formal scheme

Suppose that we have a master operator $W_R(\Gamma)$ of the form given in (33), and that this operator gives an accurate description of motion on time scales longer than Γ^{-1} . We wish to construct a projection operator $P(\Gamma - \delta\Gamma)$ which represents a good approximation to the operator $P_{\text{ex}}(\Gamma - \delta\Gamma)$ of (32), so that $W_R(\Gamma - \delta\Gamma) = P(\Gamma - \delta\Gamma)W_R(\Gamma)P(\Gamma - \delta\Gamma)$ gives an accurate description of motion on time scales longer than $(\Gamma - \delta\Gamma)^{-1}$. In addition, for the scheme to represent a renormalisation group flow, we require that $W_R(\Gamma - \delta\Gamma)$ is also of the form given in (33).

As discussed in the text, we begin by estimating an eigenmode of $W_R(\Gamma)$ that is concerned with fast motion. To achieve this, we imagine that all the rates r_α and ℓ_α are associated with very slow motion, except the triplet $\{r_\alpha, \ell_\alpha, \ell_{\alpha+1}\}$. In that case we can write the master operator as

$$W_R(\Gamma) \approx W_0 = (|P_{\alpha-1}\rangle \quad |P_\alpha\rangle \quad |P_{\alpha+1}\rangle) \begin{pmatrix} 0 & \ell_\alpha & 0 \\ 0 & -(\ell_\alpha + r_\alpha) & \ell_{\alpha+1} \\ 0 & r_\alpha & -\ell_{\alpha+1} \end{pmatrix} \begin{pmatrix} \langle Q_{\alpha-1}| \\ \langle Q_\alpha| \\ \langle Q_{\alpha+1}| \end{pmatrix} \quad (\text{A.1})$$

Diagonalising yields three eigenvalues. Since we have assumed that transitions out of site $\alpha - 1$ are very slow the ‘steady state’, i.e. the right eigenvector with eigenvalue zero, of this reduced system is simply localised on that site. Then there are two negative eigenvalues whose moduli are $\rho_{\pm} = \frac{1}{2}(r_{\alpha} + \ell_{\alpha} + \ell_{\alpha+1}) \pm \frac{1}{2}\sqrt{r_{\alpha}^2 + 2r_{\alpha}(\ell_{\alpha} + \ell_{\alpha+1}) + (\ell_{\alpha} - \ell_{\alpha+1})^2}$. These eigenvalues are associated with fast (+) and slow (−) motion. We identify ρ_+ as a rate for fast motion to the right from effective trap α . The effective dynamics proceeds by successive removal of the fastest such modes: recall (34), where ρ_+ is written as ρ_{α} . As discussed in the main text in addition to triplets of rates $(r_{\alpha}, \ell_{\alpha}, \ell_{\alpha+1})$, we also consider triplets such as $(\ell_{\alpha}, r_{\alpha}, r_{\alpha-1})$, for which the same treatment applies, with the rate λ_{α} of the fastest node given in (35). In the discussion below we assume for concreteness that the largest approximate eigenvalue among the $\{\rho_{\alpha}, \lambda_{\alpha}\}$ is $\rho_{\alpha} \equiv \rho_+$.

To accomplish the removal of the fastest mode, we will project the original master operator $W_R(\Gamma)$ onto the basis spanned by the eigenvectors associated with the slow motion. More precisely, the zero eigenvectors of the approximate master operator W_0 are $|P_{\alpha-1}\rangle$ to the right and $\langle e_3| = \langle Q_{\alpha-1}| + \langle Q_{\alpha}| + \langle Q_{\alpha+1}|$ to the left. The right and left slow eigenvectors, corresponding to eigenvalue ρ_- , we write as $|\rho_- \rangle$ and $\langle \rho_-|$. We therefore define a projection operator whose matrix elements will give the propagator on time scales longer than $1/\rho_+$:

$$\mathcal{P}_+ \equiv \sum_{\alpha'=-\infty}^{\alpha-2} |P_{\alpha'}\rangle\langle Q_{\alpha'}| + |P_{\alpha-1}\rangle\langle e_3| + |\rho_- \rangle\langle \rho_-| + \sum_{\alpha'=\alpha+2}^{\infty} |P_{\alpha'}\rangle\langle Q_{\alpha'}| \quad (\text{A.2})$$

In general, the operator $\mathcal{P}_+ W_R(\Gamma) \mathcal{P}_+$ is not of the same form as $W_R(\Gamma)$: it contains hopping processes between next-nearest neighbours for the effective traps, and does not represent a suitable approximation to $W_R(\Gamma - \delta\Gamma)$. This effect is familiar in renormalisation schemes, and requires irrelevant terms in the master equation to be discarded. In our situation, next-nearest neighbour hopping becomes irrelevant as time scales become well-separated. For example, in the barrier-like case where $r_{\alpha} \approx \ell_{\alpha+1}$ but $r_{\alpha} \gg \ell_{\alpha}$, we have

$$\begin{aligned} \mathcal{P}_+ \approx \mathcal{P}_B \equiv & \sum_{\alpha'=-\infty}^{\alpha-2} |P_{\alpha'}\rangle\langle Q_{\alpha'}| + |P_{\alpha-1}\rangle\langle Q_{\alpha-1}| + |P'\rangle(\langle Q_{\alpha}| + \langle Q_{\alpha+1}|) \\ & + \sum_{\alpha'=\alpha+2}^{\infty} |P_{\alpha'}\rangle\langle Q_{\alpha'}| \end{aligned} \quad (\text{A.3})$$

with

$$|P'\rangle = \frac{\ell_{\alpha+1}}{r_{\alpha} + \ell_{\alpha+1}} |P_{\alpha}\rangle + \frac{r_{\alpha}}{r_{\alpha} + \ell_{\alpha+1}} |P_{\alpha+1}\rangle. \quad (\text{A.4})$$

We identify $|P'\rangle$ as the right eigenvector associated with a new effective trap that combines traps α and $\alpha + 1$. The resulting master operator $\mathcal{P}_B W_R(\Gamma) \mathcal{P}_B$ is now of the same form as $W_R(\Gamma)$, with the free energy of the new effective trap given by $e^{F_{\alpha, \alpha+1}} = e^{F_{\alpha}} + e^{F_{\alpha+1}}$. Thus, we may perform an RG step by taking $\mathcal{P}(\Gamma - \delta\Gamma) = \mathcal{P}_B$ as our approximation to $\mathcal{P}_{\text{ex}}(\Gamma - \delta\Gamma)$. Such an RG step is illustrated by the transition from Fig. 3b and Fig. 3c: consistent with that figure, the transition states on either side of the new trap are unchanged during this procedure.

On the other hand, in the trap-like case where $\ell_{\alpha} \approx r_{\alpha}$ but $r_{\alpha} \gg \ell_{\alpha+1}$, we have

$$\mathcal{P}_+ \approx \mathcal{P}_T \equiv \sum_{\alpha'=-\infty}^{\alpha-2} |P_{\alpha'}\rangle\langle Q_{\alpha'}| + |P_{\alpha-1}\rangle(\langle e_3| - \langle Q'|) + |P_{\alpha+1}\rangle\langle Q'|$$

$$+ \sum_{\alpha'=\alpha+2}^{\infty} |P_{\alpha'}\rangle\langle Q_{\alpha'}| \quad (\text{A.5})$$

with

$$\langle Q'| = \frac{r_{\alpha}}{r_{\alpha} + \ell_{\alpha}} \langle Q_{\alpha}| + \langle Q_{\alpha+1}|. \quad (\text{A.6})$$

As for the previous case, $\mathcal{P}_{\text{T}}W_{\text{R}}(\Gamma)\mathcal{P}_{\text{T}}$ is of the same form as $W_{\text{R}}(\Gamma)$, so the choice $\mathcal{P}(\Gamma - \delta\Gamma) = \mathcal{P}_{\text{T}}$ corresponds to a valid RG step. In this step, trap α has been incorporated into a new effective barrier region that merges the old barrier regions $\alpha - \frac{1}{2}$ and $\alpha + \frac{1}{2}$. Its escape properties to the remaining effective traps $\alpha + 1$ and $\alpha - 1$ are described by the eigenvectors $\langle Q'|$ and $\langle e_3| - \langle Q'| = \langle Q_{\alpha-1}| + \ell_{\alpha}/(r_{\alpha} + \ell_{\alpha})\langle Q_{\alpha}|$, respectively. An example of such an RG step takes place between Figs. 3a and 3b.

It should be noted that if r_{α} is much greater than both ℓ_{α} and $\ell_{\alpha+1}$ then both (A.3) and (A.5) reduce to the case of DMF, which is $|P'\rangle = |P_{\alpha+1}\rangle$ and $\langle Q'| = \langle Q_{\alpha}| + \langle Q_{\alpha+1}|$. In practice, for any renormalisation step, we choose either to combine traps by taking $P(\Gamma - \delta\Gamma) = P_{\text{B}}$ or otherwise to combine barriers by taking $P(\Gamma - \delta\Gamma) = P_{\text{T}}$. In either case the resulting $W_{\text{R}}(\Gamma - \delta\Gamma)$ is indeed of the same form as $W_{\text{R}}(\Gamma)$: this ensures that our procedure is a valid renormalisation flow in the space of hopping models.

As discussed in Sec. 4.2, the validity of the renormalisation scheme requires that the projection operator evolves with Γ such that $\mathcal{P}(\Gamma - \delta\Gamma) \approx \mathcal{P}_{\text{ex}}(\Gamma - \delta\Gamma)$. Assuming that we combine traps α and $\alpha + 1$, we should have $\mathcal{P}_{\text{B}} \approx \mathcal{P}_{+} \approx \mathcal{P}_{\text{ex}}$. Applying perturbation theory to the fast eigenvectors, we find that corrections are small if $r_{\alpha} + \ell_{\alpha+1} \gg r_{\alpha-1}, \ell_{\alpha}, r_{\alpha+1}, \ell_{\alpha+2}$. Similarly, if we combine barriers $\alpha \pm \frac{1}{2}$, we require $\ell_{\alpha} + r_{\alpha} \gg \ell_{\alpha-1}, r_{\alpha-1}, \ell_{\alpha+1}, r_{\alpha+1}$. Essentially, if the rate r_{α} is large at a given stage of the RG (in the sense that $\rho_{\alpha} > \Gamma - \delta\Gamma$), then r_{α} must be larger than all rates in the neighbourhood, except for either ℓ_{α} or $\ell_{\alpha+1}$, one of which may be comparable to r_{α} .

Appendix A.2. Physically-motivated scheme

The formal scheme derived above differs from the one set out in the main text in the way effective traps and barriers are combined. Specifically, combining effective traps as in (A.4) would mean that an occupation probability of zero is assigned to all (integer) sites contained within the effective barrier region between the two traps. The more physical prescription (26), on the other hand, gives nonzero weights also to such sites, based on equilibration within the entire new effective trap. These prescriptions are different (except when the effective barrier region concerned consists only of single transition state), but become equivalent as long as rates are well-separated. More precisely, they are equivalent if at each RG step at least one of the three rates contributing to the largest ρ_{α} or λ_{α} is much smaller than the others. To see this, one notes that whenever an effective trap (say β) and neighbouring effective barrier (say $\beta + \frac{1}{2}$) are merged into another barrier region (say $\beta - \frac{1}{2}$), then separation of rates implies that the Boltzmann weight of trap β is much smaller (by a factor $\ell_{\beta+1}/r_{\beta}$ proportional to the small rate $\ell_{\beta+1}$) than that of trap $\beta + 1$. In the formal scheme, such traps – those that have been incorporated into effective barrier regions – are given occupation probabilities of zero in all later stages of the effective dynamics. In the physical scheme on the other hand, such traps are assigned small finite occupation probabilities whenever they form part of larger effective traps. In the limit of perfectly separated rates these small weights vanish, and the prescription (A.4) of the formal scheme is approached.

Similar comments apply to the merging of effective barriers, which in the formal scheme is done according to (A.6), while the physical scheme uses (30). The difference lies in the fact that the escape probabilities calculated from (A.6) are constant within the trap α that has been eliminated and incorporated into a larger barrier region. This corresponds to the contribution from the barrier energies $E_{i+\frac{1}{2}}$ within trap α being effectively neglected, i.e. those sites are taken to make only a small contribution to the overall free energy of the barrier. Again this can be shown to be only a negligible difference to the physical scheme in the limit of well-separated rates.

Overall, given that the two schemes both respect the duality relations between hopping models (see Sec. 4.4) and that they become equivalent in the limit of well-separated rates in which they can be justified, we prefer to use the scheme described in the main text because it corresponds more closely to physical intuition. In contrast to the formal scheme, it does require that we retain the bare master operator at all stages, in order to be able to update free energies when traps and barriers are combined, but the computational overhead for this is negligible.

References

- [1] M. D. Ediger, *Annu. Rev. Phys. Chem.* **51**, 99 (2000); E. R. Weeks *et al.*, *Science* **287**, 627 (2000); W. Kegel and A. van Blaaderen, *Science* **287**, 290 (2000).
- [2] M. T. Cicerone, P. A. Wagner, and M. D. Ediger, *J. Phys. Chem. B* **101**, 8727 (1997); R. Yamamoto and A. Onuki, *Phys. Rev. Lett.* **81**, 4915 (1998); C. Donati *et al.*, *Phys. Rev. E* **60**, 3107 (1999); B. Doliwa and A. Heuer, *Phys. Rev. E* **67**, 030501 (2003); Y. Jung, J. P. Garrahan and D. Chandler, *Phys. Rev. E* **69**, 061205 (2004).
- [3] See, for example, M. J. Saxton and K. Jacobson, *Annu. Rev. Biophys. Biomol. Struct.* **26**, 373 (1997); M. Weiss *et al.*, *Biophys. J.* **87**, 3518 (2004); D. S. Banks and C. Fradin, *Biophys. J.* **89**, 2960 (2005); I. Golding and E. Cox, *Phys. Rev. Lett.* **96**, 098102 (2006); M. A. Lomholt, I. M. Zaid and R. Metzler, *Phys. Rev. Lett.* **98**, 200603 (2006).
- [4] J. Bernasconi *et al.*, *Phys. Rev. Lett.* **42**, 819 (1979).
- [5] E. Bertin, J.-P. Bouchaud and F. Lequeux, *Phys. Rev. Lett.* **95**, 015702 (2005); R. L. Jack, P. Sollich and P. Mayer, *Phys. Rev. E* **78**, 061107 (2008).
- [6] S. Alexander *et al.*, *Rev. Mod. Phys.* **53**, 175 (1981).
- [7] S. Havlin and D. Ben Avraham, *Adv. Phys.* **36**, 695 (1987).
- [8] J.-P. Bouchaud and A. Georges, *Phys. Rep.* **195**, 127 (1990).
- [9] R. Metzler and J. Klafter, *Phys. Rep.* **339**, 1, (2000).
- [10] R. L. Jack and P. Sollich, *J. Phys. A* **41**, 324001 (2008).
- [11] P. le Doussal, C. Monthus and D. S. Fisher, *Phys. Rev. E* **59**, 4795 (1999).
- [12] See, for example, D. J. Wales, M. A. Miller and T. R. Walsh, *Nature* **394**, 758 (1998); F. Stillinger, *Science* **267**, 1935 (1995).
- [13] J. Machta, *J. Phys. A* **18**, L531 (1985).
- [14] C. Monthus and J.-P. Bouchaud, *J. Phys. A* **29**, 3847 (1996).
- [15] E. Bertin and J.-P. Bouchaud, *Phys. Rev. E* **67**, 026128 (2003).
- [16] C. Monthus, *Phys. Rev. E* **68**, 036114 (2003).
- [17] S. Tanase-Nicola and J. Kurchan, *Phys. Rev. Lett.* **91**, 188302 (2003); S. Tanase-Nicola and J. Kurchan, *J. Stat. Phys.* **116**, 1201 (2004).
- [18] J. Zinn-Justin, *Quantum Field Theory and Critical Phenomena*, chapter 17 (Oxford University Press, Oxford, 2002).
- [19] J. Tailleur, J. Kurchan and V. Lecomte, *J. Phys. A* **41**, 505001 (2008).
- [20] R. L. Jack and P. Sollich, in preparation.
- [21] P. J. H. Denteneer and M. H. Ernst, *Phys. Rev. B* **29**, 1755 (1984).
- [22] Y. G. Sinai, *Theor. Prob. Appl.* **27**, 247 (1982).
- [23] B. Gaveau and L. S. Schulman, *J. Math. Phys.* **39**, 1517 (1998); see also G. Biroli and J. Kurchan, *Phys. Rev. E* **64**, 016101 (2001); A. Bovier *et al.*, *Commun. Math. Phys.* **228**, 219 (2002).